

SPG Mitteilungen Communications de la SSP

Auszug - Extrait

Progress in Physics (98)

THz frequency combs for integrated coherent photonics

Giacomo Scalari ¹ (scalari@phys.ethz.ch), Urban Senica ¹, Andres Forrer ¹, Paolo Micheletti ¹, Tudor Olariu ¹, Sara Cibella ², Guido Torrioli ², Mattias Beck ¹, Jérôme Faist ¹

¹ Quantum Optoelectronics Group, Institute of Quantum Electronics, ETH Zürich, CH-8093 Zürich

² Istituto di Fotonica e Nanotecnologie, CNR, Via del Fosso del Cavaliere 100, IT-00133 Rome

Progress in Physics (98)

THz frequency combs for integrated coherent photonics

Giacomo Scalari¹ (scalari@phys.ethz.ch), Urban Senica¹, Andres Forrer¹, Paolo Micheletti¹, Tudor Olariu¹, Sara Cibella², Guido Torrioli², Mattias Beck¹, Jérôme Faist¹

¹ Quantum Optoelectronics Group, Institute of Quantum Electronics, ETH Zürich, CH-8093 Zürich

² Istituto di Fotonica e Nanotecnologie, CNR, Via del Fosso del Cavaliere 100, IT-00133 Rome

1 Introduction

Recently, there has been a growing interest in integrated THz photonics for various applications in communications, spectroscopy and sensing [1, 2]. We discuss here the fundamental aspects and some experimental realizations of on-chip THz frequency combs based on semiconductor heterostructures. An optical frequency comb [3] is an optical source with a spectrum constituted by a set of modes which are perfectly equally spaced and have a well-defined phase relationship between each other. As a result, the ensemble of comb frequency lines at frequencies f_n , given by:

$$f_n = f_{ceo} + n f_{rep} \quad (1)$$

are spaced by the repetition rate of the laser f_{rep} which can be made extremely stable and locked to an external microwave source. In addition, the ensemble of frequency lines can be shifted by the so-called carrier-envelope offset frequency f_{ceo} [3]. For applications in sensing and spectroscopy, as well as for next generation telecom data links, the availability of on-chip frequency combs is of paramount importance [4].

As shown schematically in Fig. 1(a), optical comb generation is relying on the combination of three elements: an optical cavity, (either a Fabry-Perot as displayed or a ring cavity), a gain medium to reach threshold and a non-linear element, usually a saturable absorber. These three functions are neatly combined in traditional pulsed mode-locked lasers [8] which were the first used to generate optical frequency combs. In a chip-based cavity, optimally the two functions, gain and non-linearity, are combined in the same material. Optical frequency combs have recently been generated using high-Q microcavity resonators pumped by narrow linewidth continuous wave lasers, Fig. 1(b) [9, 10]. Here, the Kerr non-linearity is responsible for establishing the stable phase relationship between the laser modes and the gain for the comb modes. In contrast to mode-locked lasers, Kerr combs can exhibit complex phase relations between modes that do not correspond to the emission of single pulses [11]. Quantum Cascade Lasers (QCLs) [12] are semiconductor injection lasers emitting throughout the

mid-infrared (3 - 24 μm) and THz (50 - 250 μm) [13, 14] regions of the electromagnetic spectrum. First demonstrated in 1994 [15] in the mid-infrared and 2002 in the THz [16], they have undergone a tremendous development. Their capability to operate in a very wide frequency range makes them very convenient devices for optical sensing applica-

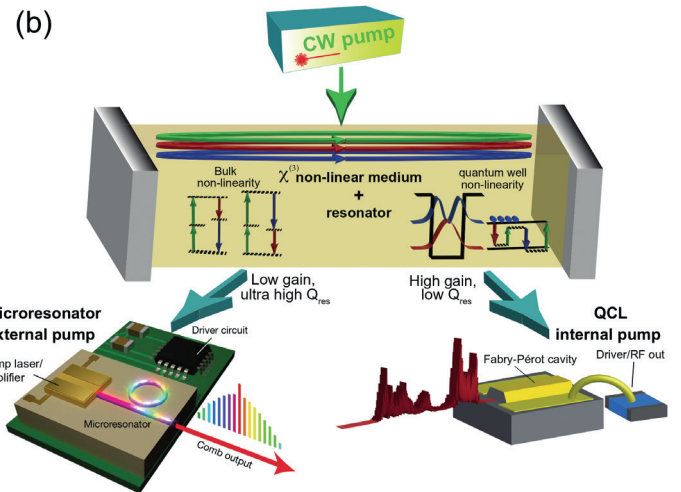
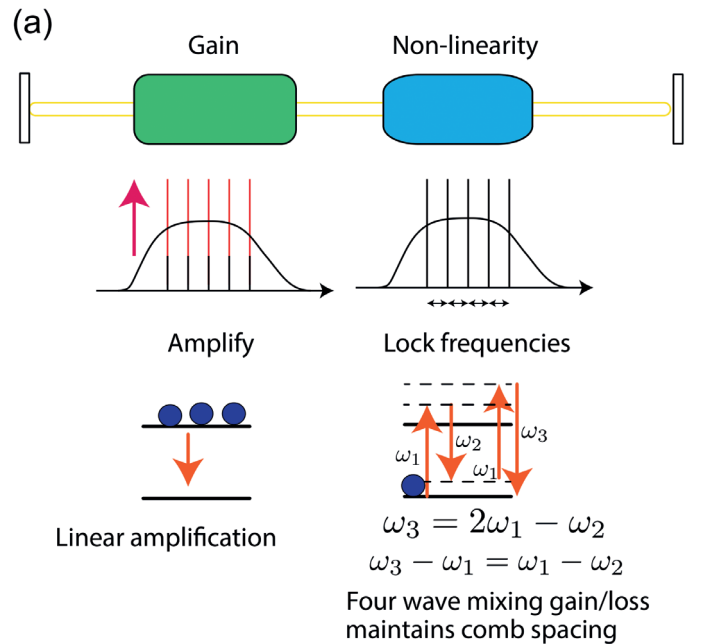


Figure 1: Schematic functional building blocks of an optical frequency comb generator. (a) The gain section brings the equidistant modes of a cavity above threshold while the fast non-linear section locks the mode separation via four wave mixing. (b): In an integrated version, the gain and non-linearity can be combined together in a single element. In a QCL, the gain provides the non-linearity while in microresonator combs the non-linear section provides also the gain via optical pumping. Figures adapted from [5, 6]. (c): Experimental scheme for SWIFT spectroscopy (adapted from [7]): the two quadratures, demodulated at the repetition frequency ν_{rep} , yield the intermodal phase differences $\Delta\varphi_n$.

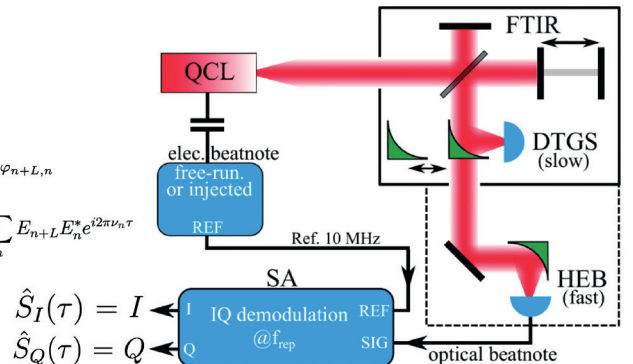
(c)

$$S_{+,L}^{(n)} = |E_{n+L}| |E_n| e^{i\Delta\varphi_{n+L,n}}$$

$$\hat{S}_{+,L}(\tau) = \hat{S}_I(\tau) + i\hat{S}_Q(\tau) = \sum_n E_{n+L} E_n^* e^{i2\pi\nu_n\tau}$$

$$\hat{S}_I(\tau) = I$$

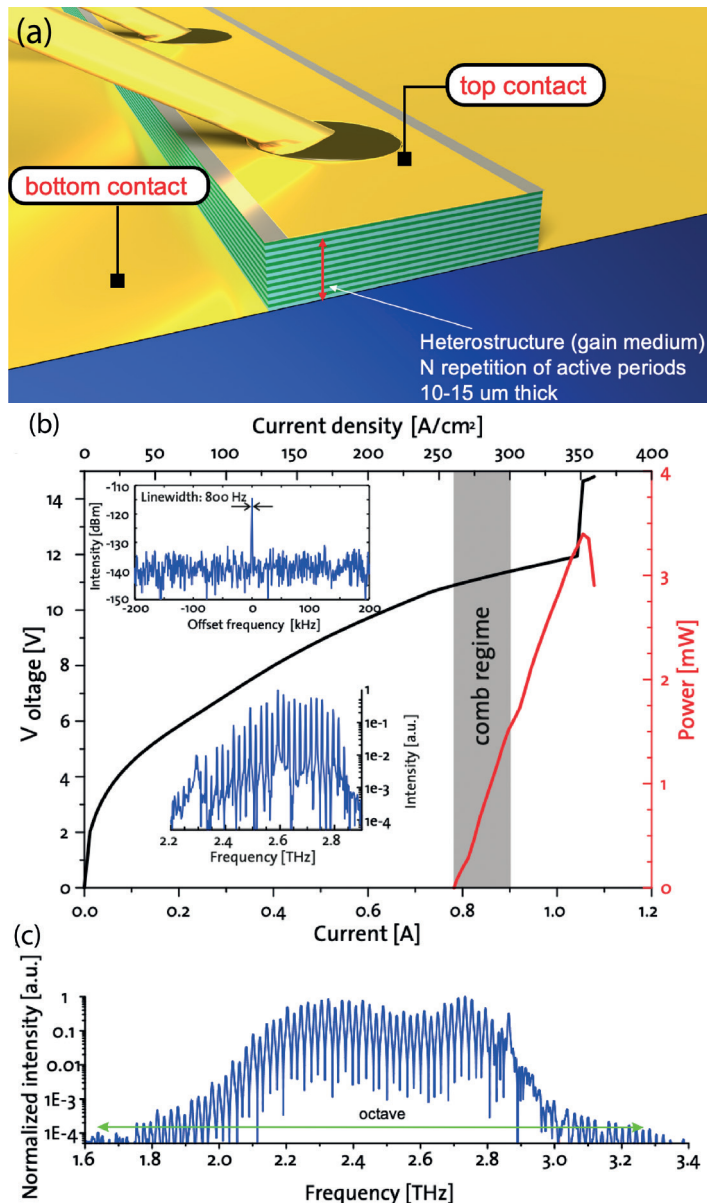
$$\hat{S}_Q(\tau) = Q$$



tions. The ultrafast nature and designer capabilities of the gain medium are essential ingredients for the operation of these lasers as frequency combs.

2 QCL comb operation

It was suggested very early that broadband QCLs could be mode-locked to provide ultrashort mid-infrared pulses [17]. Quantum cascade lasers, being based on intersubband transitions in quantum wells, exhibit ultrafast upper state lifetimes with values in the picosecond range ($\tau \approx 40 - 0.6$ ps depending on the operating frequency and design). These times are much shorter than the typical cavity round trip time τ_{rt} (64 ps for a 3 mm long device), such that the product $\omega\tau_2 \ll 1$, where $\omega = 2\pi/\tau_{rt}$ is the angular frequency corresponding to the longitudinal mode spacing. As a result, passive mode-locking resulting in short pulse formation is highly disfavoured. For some THz QCLs, lifetimes can be significantly longer, up to 40 ps [18] such that the product $\omega\tau_2$ can be close to unity. At the same time, the very short upper state lifetime, that strongly hinders fundamental mode-locking, is responsible for a very broadband four wave mixing process, whose bandwidth is much larger than in the case of interband semiconductor lasers that display significantly longer upper state lifetimes. The first observation of QCL comb operation was reported by Hugi et al.,



[19]: from there on an increasing number of experimental [20] and theoretical papers [21, 22] showed that, at least for Mid-IR QCLs, the inter-modal phases are quadratically dispersed, corresponding to an instantaneous frequency that is linearly chirped, as in an FM locked laser [23]. Several theory papers contributed to elucidate the underlying physics showing the intimate connection between the comb generation in QCLs with the Ginzburg-Landau equation [21, 24] and with phase solitons [25].

To investigate the comb states and properties of the QCL emission, since generally QCL comb operation does not correspond to optical pulses, specific characterization techniques had to be developed in order to assess the comb coherence and reconstruct its time-domain profile. SWIFT (Shifted Wave Interference Fourier Transform) spectroscopy, pioneered by D. Burghoff [26, 27], gives direct access to the relative phases between two modes. It consists of demodulating the laser signal filtered by the FTIR at the roundtrip frequency. This necessitates the use of very fast optical detectors (\approx GHz range). A schematic of the experimental setup is visible in Fig.1(c), together with the expressions for the measured signals.

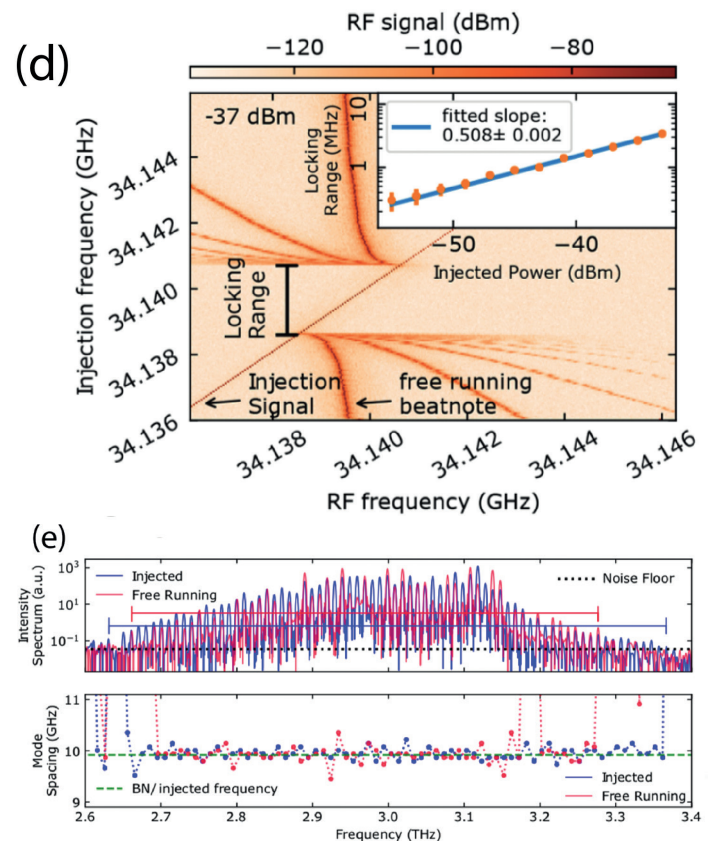


Figure 2: (a): schematic of a THz QCL processed in a double-metal waveguide Fabry-Perot resonator. (b): Light-current-voltage characteristics of a heterogeneous QCL emitting on a comb state for the first 100 mA of the IV curve (grey area). Inset: RF beatnote and spectrum of the comb at $T = 25$ K. (c) Octave spanning spectrum (not comb) of the device at $I = 1$ A (adapted from [29]). (d): Injection locking map for 37 dBm for a homogeneous THz QCL. Inset: Locking range for different injection powers following the square-root dependence of the Adler's equation (adapted from [34]). (e): Free running (single beatnote regime) and RF strong injected spectra at 80 K. Significant change in the modes as well as generation of additional modes due to injection which leads to a spectral bandwidth from 600 GHz to 700 GHz. Mode spacing showing a quantitative agreement of the equally spaced modes (adapted from [35]).

Looking at the first THz QCL comb demonstrations, these devices have been driven in the comb regime by careful dispersion compensation [28], by engineering a broadband QCL with a flat gain curve [29, 30] and by a combination of both elements [31]. It was recently shown that it is possible to achieve octave-spanning lasers at THz frequencies using QCLs [29], Fig. 2(c). This very wide frequency coverage is possible due to the mentioned gain engineering capability typical of intersubband transitions coupled to the extremely broadband nature of the double-metal waveguide. THz QCLs generally operate in double-metal cavities where the waveguide claddings are constituted by two metallic layers, Fig. 2(a) [32, 14], as in a microwave microstrip resonator. For the fundamental TM-polarized optical mode that is generated in the cavity, there is no cutoff frequency, enabling ultra-broadband operation. As discussed above the broad gain results in a group velocity dispersion (GVD) which is low in value and relatively constant with frequency. Furthermore the used double metal waveguides introduce only a small amount of GVD to the laser. Therefore these lasers can act as frequency combs similar as mid-infrared QCL combs. The characteristics of such a THz QCL comb are displayed in Fig. 2(b). The shown comb has 1.55 mW of output power while spanning over a spectral bandwidth of 507 GHz. The beatnote has a linewidth of 800 Hz which is still jitter-limited since the laser is not actively stabilized. Last developments of wide bandwidth THz QCL comb based on multi-stack active cores show an impressive bandwidth coverage of 1.1 THz at 30 K ($\frac{\Delta f}{f} = 36\%$) [33] and 700 GHz at 80 K under RF injection from an homogeneous structure [34, 35] (see Fig.2 (d,e)).

3 THz QCL combs on a planarized platform

Integrated photonics [36] makes extensive use of on-chip optical elements such as sources, splitters, modulators, and high-confinement waveguides embedded in a planar platform to efficiently process and route optical signals. In the THz frequency range, a prominent candidate for source integration is the THz quantum cascade laser [37]. In more

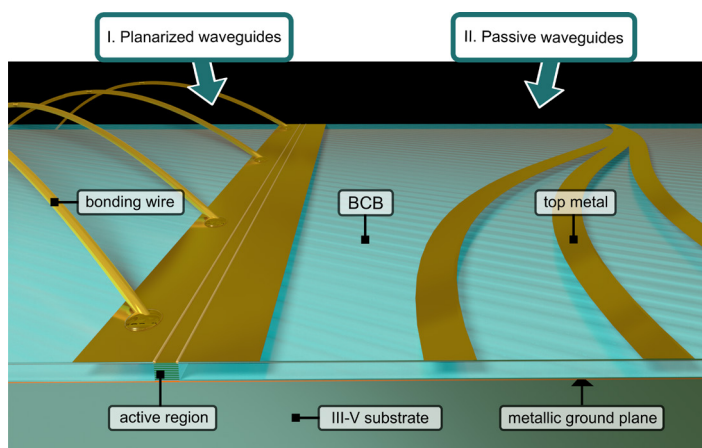


Figure 3: Schematic of platform for broadband coherent THz photonics based on planarized active and passive waveguides embedded in BCB, a low-loss polymer. I. The planarized active waveguide consists of a standard double metal waveguide encompassed in BCB and an extended top contact metallization, enabling narrower active ridge geometries and providing bonding pads. II. Passive waveguides can also be fabricated, consisting of metallic stripes on top of BCB, which provide confinement and guide the optical mode. These can be used to co-integrate active and passive elements on the same chip. (Figure adapted from [7].)

complex photonic systems [38], some of the crucial features for laser integration [39] are the reduction of the electrical consumption, and consequently of the injected current, and the efficient coupling to low-loss passive waveguides. In this section we discuss our approach to integrated THz photonics that allows signal propagation with passive elements and coherent source integration for applications such as broadband sensing [40] and coherent telecommunications [41]. We leverage on the presence of a common metallic ground plane to demonstrate the integration of several active and passive THz photonic components onto the same semiconductor platform, allowing for efficient signal processing at THz and RF frequencies. We employ a low-loss polymer BCB, which has been used before for narrowband devices such as THz photonic crystal QCLs [42] and antenna-coupled QCLs [43]. In our work, we focus on broadband and comb devices, highlighting improved performance in several crucial figures of merit such as dispersion, RF and thermal properties, and demonstrating the co-integration of active and passive elements on the same photonic chip. The basic building block is a high-performance planarized double-metal waveguide with an extended top metallization, as shown in Fig. 3.

Following a standard double metal waveguide fabrication process [44] with dry-etched active region waveguides, a microelectronic-grade low-loss polymer Benzocyclobutene (BCB) is spin-coated and baked as the surrounding material. The latter is widely used in microelectronics and has already been successfully employed in several THz applications [43, 45]. Following planarization, an extended top metallization is deposited over the active region and the BCB-covered area on the sides, which offers several advantages, as discussed below. From the active region standpoint, for these first demonstrations we used a strongly diagonal, low-threshold broadband GaAs/AlGaAs heterostructure, fully described in [34].

In the context of THz frequency combs, it has been shown that the control over transverse modes is essential in order to obtain a regular and flat-top comb spectrum [46]. The introduction of side absorbers mitigates lasing in higher-order transverse modes due to increased waveguide losses. A similar result can be achieved by reducing the transverse dimension of the laser ridge to 50 μm and below. However, for conventional double metal ridges, the width cannot be arbitrarily small since the waveguides are usually contacted by wire bonding directly on the top metallic cladding. This inherently limits the effective ridge width w to the dimensions of the bonding wire patch, making devices with ridges of 50 μm or below challenging to contact and prone to failures. With planarization the bonding wires can be placed on top of the extended top metallization over the passive, BCB-covered area, preventing formation of any defects or local hotspots on top of the active region, and enabling the fabrication of very narrow waveguides, well below the bonding wire size ($\approx 30 \mu\text{m}$). The narrow waveguide width can be employed as an efficient selection mechanism for the fundamental transversal lasing mode, and is also beneficial for heat dissipation and high temperature continuous wave (CW) operation. With reduced waveguide widths we enter the regime of “wire” lasers [47], which have a very favourable figure of merit for their surface-to-volume ratio as it scales as the inverse of the width $S/V \propto 1/w$, reducing the

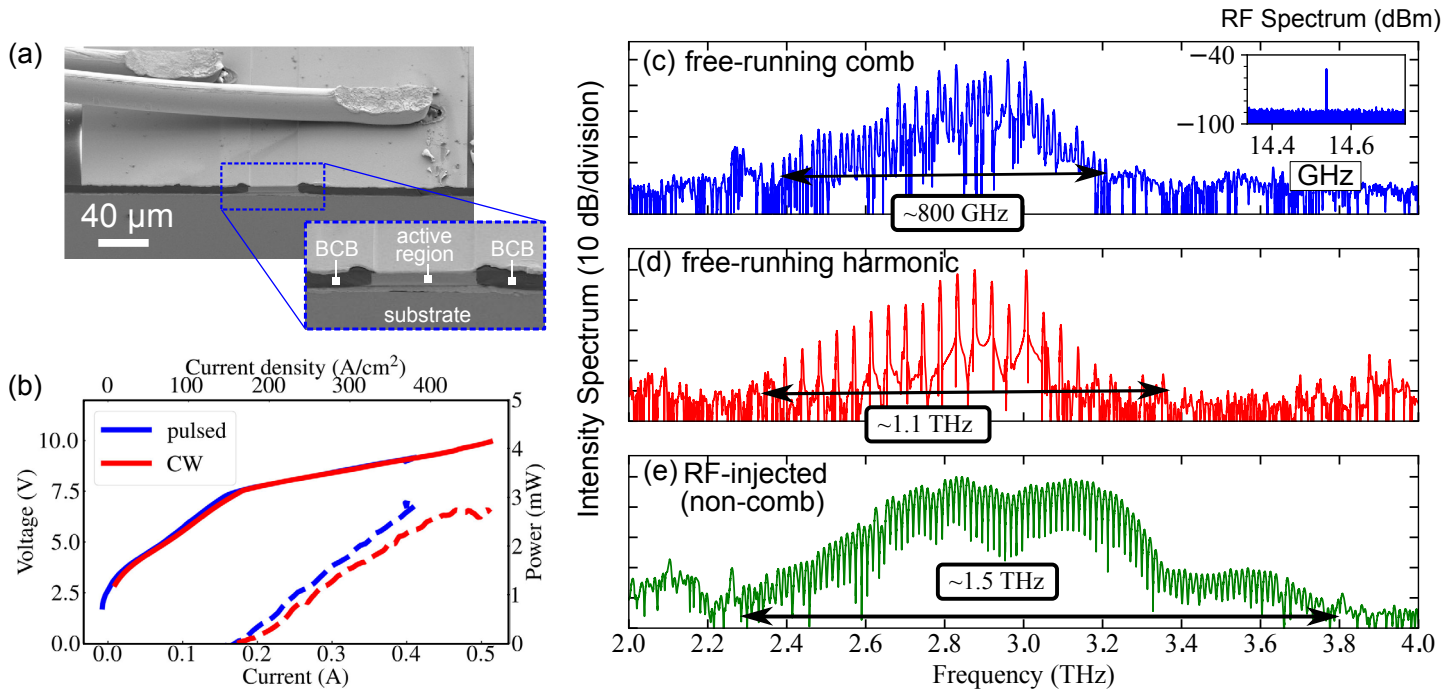


Figure 4: (a) SEM image of a planarized, 40 μm wide ridge waveguide device, showing the cleaved front facet. The bonding wires are placed on the extended top metallization over the BCB-covered area. (b) LIV curves of a ridge laser sample measured in pulsed mode (500 ns pulses, 10 % duty cycle) and in CW at a heatsink temperature of 40 K. (c) A free-running frequency comb spanning around 800 GHz, with the measured single strong RF beatnote (-55 dBm) shown in the inset. (d) A broadband free-running third harmonic state, covering a bandwidth of 1.1 THz. (e) With strong RF injection (+32 dBm at source) close to the free-running mode spacing, the emission spectrum can be broadened, spanning around 1.5 THz. (Figure adapted from [7].)

heating inside the active region waveguide.

One major advantage of using double metal waveguides is the large overlap factor of the propagating mode, reaching nearly unity. It can, however, reduce with the waveguide width. Finite element simulations [7] show that computed overlap factor remains above 90 % for ridge widths of above 20 μm for both the standard and planarized waveguides at a frequency of 3 THz. Since we are interested in frequency combs, an important figure of merit is the GVD of the waveguide. The calculated dispersion of the planarized waveguides is indeed significantly reduced with respect to the standard ones, especially at low (< 3 THz) frequencies. This is related to the change of the modal overlap factor as a function of frequency, as the evanescent field distribution changes differently for the standard and planarized waveguides.

We employ planarized ridges with a width of 40 μm , narrow enough for fundamental transversal mode selection, and wide enough for a large overlap factor and low propagation losses. In Fig. 4(a) we show an SEM image of the front part of the ridge waveguide with a cleaved facet and DC bonding wires on the extended top metallization.

Light-current-voltage (LIV) characteristics, shown in Fig. 4(b), display a low threshold current density in the order of 140 A/cm^2 at a heat sink temperature of 40 K, which is due to the low-loss Cu-Cu planarized waveguide and the low-dissipation superdiagonal active region [34]. These planarized devices typically operate up to around 115 K in continuous wave (CW). We examine now the comb properties of free-running devices: a typical measurement result is shown in Fig. 4(c), where the THz spectrum spans around 800 GHz and there is a single stable RF beatnote at the cavity repetition rate f_{rep} . The measured free-running

RF beatnotes in planarized waveguides can reach relatively high powers of -60 to -55 dBm at the spectrum analyzer readout, indicating improved RF properties. As a comparison, typical beatnote intensities for standard double metal waveguides with similar dimensions processed on the same epilayer usually reach values of around -70 dBm. Moreover, self-starting pure harmonic states [48, 49] (Turing patterns) can be observed at specific bias points, where the mode spacing is an integer multiple of the fundamental f_{rep} [50]. A typical harmonic state spectrum spanning over 1.1 THz is shown in Fig. 4(d), in this case corresponding to the third harmonic. By injecting an external RF signal to the laser cavity, it is possible to strongly modify the lasing operation both of a comb state [51, 52] or also of a high phase noise state [34, 53]. In Fig. 4(e) we show an example where injecting a strong RF signal (+32 dBm at source) close to the natural cavity mode spacing ($f_{\text{rep}} \pm \pm 200$ MHz) can broaden the THz emission spectrum to over 1.5 THz. These are usually not frequency comb states due to the limiting chromatic dispersion over such a wide bandwidth, but still very useful as sources of broadband THz radiation. In order to assess the comb coherence and retrieve the phase between adjacent modes for reconstructing the time-domain emission profile, we used Shifted Wave Interference Fourier Transform Spectroscopy (SWIFTS) [26, 54]. A hot electron bolometer (HEB) [55] was used as the fast detector. Mounting and antenna-coupling have been optimized to enhance RF performance [56]. When illuminated with a THz QCL frequency comb, the optical beatnote generated between adjacent THz modes can be measured directly on the bias line of the detector and fed into a spectrum analyzer.

We now discuss two measurement examples in two different regimes. First, we analyze the comb state of a ridge waveguide device, injection-locked to the natural $f_{\text{rep}} = 14.540$ GHz with a relatively weak RF signal (+5 dBm at the source)

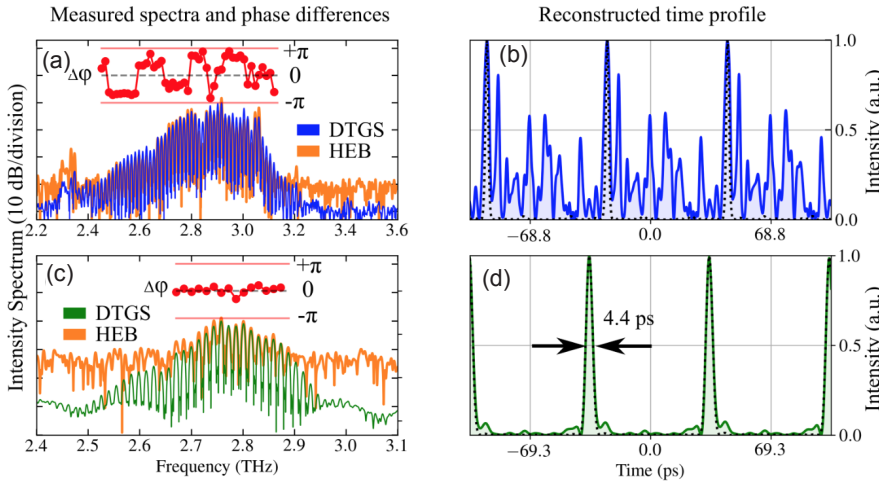


Figure 5: (a, b) Measurements of a weakly-injected (+5 dBm) device show scattered phase differences, and the reconstructed time profile has a quasi-continuous periodic output intensity. (c, d) Strong RF injection (+32 dBm) close to the repetition rate frequency on a ridge device close to lasing threshold results in active mode locking, producing pulses as short as 4.4 ps (close to the Fourier limit, dotted line). (Figure adapted from [7].)

in order to stabilize the repetition rate. The measured spectra and relative phases are shown in Fig. 5(a), where the THz spectral product measured with a slow DTGS detector (blue) and the HEB (orange) have a good overlap and comparable signal-to-noise ratio, which is attributed to the high coherence of the comb state. The extracted relative phases are scattered across different values (with some mode groups sharing the same phase), which also depends on the amplitude of the injected RF signal. The reconstructed time profile produces a quasi-continuous periodic output with some amplitude modulation, as shown in Fig. 5(b). The second example is the same ridge waveguide device operating just above lasing threshold and driven by a strong RF injection (+32 dBm at the source) at $f_{inj} = 14.538$ GHz, close to the natural repetition rate $f_{rep} = 14.540$ GHz. The measurement results in Fig. 5(c) show that we can reach an active mode locking regime [57, 58], where all the measurable modes have a flat phase profile, and the reconstructed time profile in Fig. 5(d) is a train of nearly Fourier-limited pulses as short as 4.4 ps. Since only the central high-intensity modes could be measured with the HEB detector, the actual emitted THz pulses are very likely even shorter (assuming all the modes on the spectrum tails have the same phase).

As a further point of interest, the possibility to planarize the etched structures allows to engineer the waveguide dispersion in order to produce regions of anomalous dispersion that can be exploited with ring resonators for the generation of temporal solitons. We recently succeeded in this endeavour observing THz solitons at 2.8 THz from a double-ring quantum cascade laser [59].

4 Passive waveguide components

Another important advantage of our planarized platform is the possibility to co-integrate

active and passive elements. While we have already demonstrated planar reflective and outcoupling passive antenna structures [43, 60], here we designed passive waveguides for on-chip signal routing between various elements. Integration of passive waveguides is critical in the development of an integrated photonic platform. Near-infrared photonic circuits are nowadays a reality, and a similar approach can be envisioned for THz frequencies. An optical microscope image of a fabricated device is shown in Fig. 6(a), where an active ridge is connected to straight and bent passive waveguides on each side. The passive waveguide is a metallized stripe on top of BCB which continues beyond the active region waveguide. The active waveguide has a width of 40 μm , while the passive waveguides have a slightly larger width of 60 μm to prevent any leakage to the sides due to possible lithographic misalignment. The minimum bending radius of the bent waveguide section is around $R = 500$ μm . Full-wave 3D numerical simulations show that the optical mode is guided below the metal stripe, following also non-straight paths (Fig. 6(a,b)). The reflectivity (coupling efficiency) at the active/passive waveguide interface can be tuned by the shape of the active and passive waveguides. In the simplest case of a flat (dry-etched) active waveguide facet, a reflectivity of $R = |S_{11}|^2 = 22.5\%$ into the fundamental active waveguide mode, and a transmission of $T = |S_{21}|^2 = 57.0\%$ into the fundamental passive waveguide mode is obtained from a 3D numerical simulation at a frequency of 3 THz. This gives an

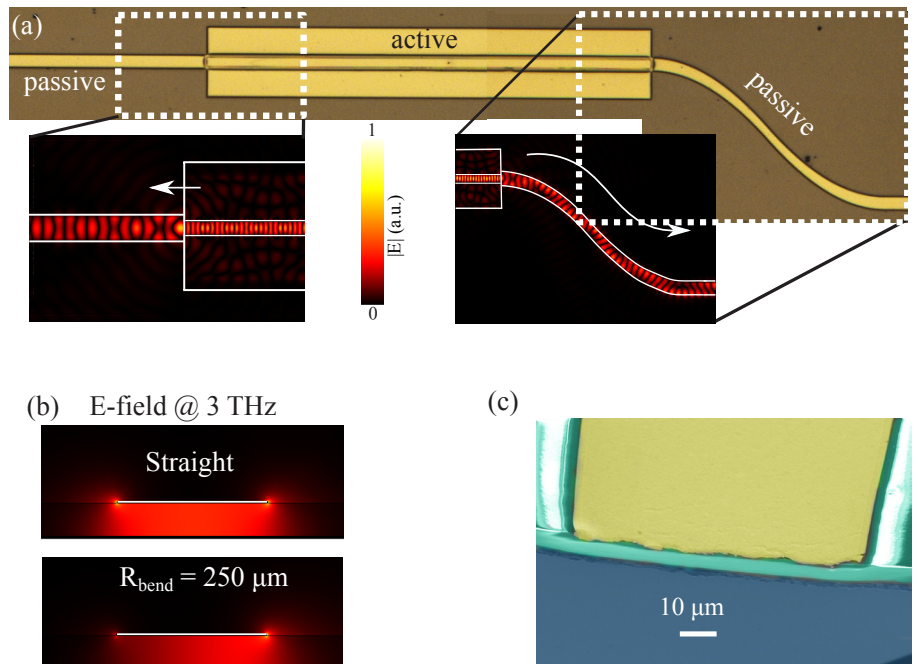


Figure 6: (a) Optical microscope image of a ridge device co-integrated with straight and curved passive waveguide elements, consisting of a metallized stripe on top of BCB. Insets show the simulated THz wave propagation with minimal scattering and bending losses at 3 THz. (b) Simulated electric field distribution in the passive waveguide cross-section at 3 THz. In the case of a straight waveguide, the intensity is concentrated symmetrically below the metal stripe, while it shifts to the outer side in the case of a bent path. (c) False color SEM images of the cleaved passive waveguide with a flat BCB end facet. Figure adapted from [7].

insertion loss of $L_{ins} = 1 - \frac{T}{1-R} = 26.5\% = 1.34$ dB. By using different combinations of cleaved and passive waveguide facets (see Fig.6(c)), the planarized geometry offers the possibility to change the cavity reflectivity, adding an important element to the comb engineering toolbox. This could be expanded further by fabricating more complex dry-etched waveguide facet geometries, for example an adiabatic taper coupled to a passive waveguide, to make the reflectivity even lower. Finally, coupling broadband frequency combs to passive waveguides on the same chip, as already demonstrated in the Mid-IR [61], is an important milestone towards fully integrated active and passive THz photonic circuits and spectrometers.

5 Conclusions

We discussed THz quantum cascade lasers frequency combs covering the frequency range 2 - 3.5 THz. They naturally provide comb operation in a mixed AM-FM state. They can be driven in a full AM operation with pulses as short as a few ps by RF injection. Especially in the case of the planarized devices, the extended top contact metallization enables bonding wires to be placed over the BCB-covered area, which results in low waveguide losses, improved dispersion, RF and thermal dissipation properties, and allows for an independent design of THz and RF waveguide properties. The fabrication of narrow waveguides acts as a fundamental mode selection mechanism and further improves heat dissipation. Free-running broadband frequency combs over 800 GHz and harmonic states over 1.1 THz are observed. The co-integration of passive elements with custom on-chip guiding, reflection and outcoupling properties makes such a platform extremely promising for a number of applications, from spectroscopy and sensing to local area network communications.

The authors gratefully acknowledge funding from the ERC Grant CHIC (No. 724344) and from SNF MINT project n. 200021 – 212735.

References

- [1] M. Smit, K. Williams, and J. van der Tol, *APL Photonics* **4**, 050901 (2019).
- [2] K. Sengupta, T. Nagatsuma, and D. M. Mittleman, *Nature Electronics* **1**, 622 (2018).
- [3] T. Udem, R. Holzwarth, and T. Hansch, *Nature* **416**, 233 (2002).
- [4] L. Chang, S. Liu, and J. Bowers, *Nature Photonics* **16**, 95 (2022).
- [5] G. Scalari, J. Faist, and N. Picqué, *Applied Physics Letters* **114**, 150401 (2019).
- [6] D. Botez and M. Belkin, *Mid-Infrared and Terahertz Quantum Cascade Lasers*, Cambridge University Press, 2023.
- [7] U. Senica et al., *Light: Science & Applications* **11**, 347 (2022).
- [8] H. A. Haus, *IEEE J. Sel. Top. Quantum Electron.* **6**, 1173 (2000).
- [9] P. Del'Haye et al., *Nature* **450**, 1214 (2007).
- [10] T. J. Kippenberg, R. Holzwarth, and S. A. Diddams, *Science* **332**, 555 (2011).
- [11] P. Del'Haye, K. Beha, S. B. Papp, and S. A. Diddams, *Physical Review Letters* **112**, 043905 (2014).
- [12] J. Faist, *Quantum cascade lasers*, Oxford University Press, 1st edition, 2013.
- [13] R. Köhler et al., *Nature* **417**, 156 (2002).
- [14] G. Scalari et al., *Laser & Photonics Reviews* **3**, 45 (2009).
- [15] J. Faist et al., *Science* **264**, 553 (1994).
- [16] R. Köhler et al., *Nature* **417**, 156 (2002).
- [17] C. Gmachl, D. Sivco, R. Colombelli, F. Capasso, and A. Cho, *Nature* **415**, 883 (2002).
- [18] C. G. Derntl et al., *Applied Physics Letters* **113**, 181102 (2018).
- [19] A. Hugi, G. Villares, S. Blaser, H. C. Liu, and J. Faist, *Nature* **492**, 229 (2012).
- [20] M. Singleton, P. Jouy, M. Beck, and J. Faist, *Optica* **5**, 948 (2018).
- [21] N. Opačák and B. Schwarz, *Physical Review Letters* **123**, 243902 (2019).
- [22] C. Silvestri, L. L. Columbo, M. Brambilla, and M. Gioannini, *Optics Express* **28**, 23846 (2020).
- [23] A. E. Siegman, *Lasers*, University Science Books, Mill Valley, California, USA, 1986.
- [24] M. Piccardo et al., *Nature* **582**, 360 (2020).
- [25] D. Burghoff, *Optica* **7**, 1781 (2020).
- [26] D. Burghoff et al., *Nature Photonics* **8**, 462 (2014).
- [27] D. Burghoff et al., *Optics Express* **23**, 1190 (2015).
- [28] D. Burghoff et al., *Nature Photonics* **8**, 462 (2014).
- [29] M. Rösch, G. Scalari, M. Beck, and J. Faist, *Nature Photonics* **9**, 42 (2015).
- [30] M. Wienold, B. Röben, L. Schrottko, and H. T. Grahn, *Opt. Express* **22**, 30410 (2014).
- [31] F. P. Mezzapesa et al., *Optics Express* **27**, 20231 (2019).
- [32] B. S. Williams, *Nature Photonics* **1**, 517 (2007).
- [33] M. Roesch et al., *Nanophotonics* **7**, 237 (2018).
- [34] A. Forrer et al., *ACS Photonics* **7**, 784 (2020).
- [35] A. Forrer, L. Bosco, M. Beck, J. Faist, and G. Scalari, *Photonics* **7** (1), 9 (2020).
- [36] D. Thomson et al., *Journal of Optics* **18** (2016).
- [37] R. Köhler et al., *Nature* **417**, 156 (2002).
- [38] M. Piccardo et al., *Journal of Optics* **24**, 013001 (2022).
- [39] G. Roelkens et al., *Laser & Photonics Reviews* **4**, 751 (2010).
- [40] L. Consolino et al., *Communications Physics* **3**, 69 (2020).
- [41] S. Koenig et al., *Nature Photonics* **7**, 977 (2013).
- [42] H. Zhang, L. A. Dunbar, G. Scalari, R. Houdré, and J. Faist, *Optics Express* **15**, 16818 (2007).
- [43] L. Bosco et al., *Appl. Phys. Lett* **109**, 201103 (2016).
- [44] B. S. Williams, *Nature Photonics* **1**, 517 (2007).
- [45] E. Perret, N. Zerounian, S. David, and F. Aniel, *Microelectronic Engineering* **85**, 2276 (2008).
- [46] D. Bachmann et al., *Optica* **3**, 1087 (2016).
- [47] M. I. Amanti, G. Scalari, F. Castellano, M. Beck, and J. Faist, *Optics Express* **18**, 6390 (2010).
- [48] D. Kazakov et al., *Nature Photonics* **11**, 789 (2017).
- [49] D. Burghoff, *Optica* **7**, 1781 (2020).
- [50] A. Forrer et al., *Applied Physics Letters* **118**, 131112 (2021).
- [51] B. Schneider et al., *Laser & Photonics Reviews* **15** (2021).
- [52] J. Hillbrand, A. M. Andrews, H. Detz, G. Strasser, and B. Schwarz, *Nature Photonics* **13**, 101 (2019).
- [53] P. Gellie et al., *Optics Express* **18**, 20799 (2010).
- [54] D. Burghoff, D. Ren, and Z. Han, *Optics Express* **28**, 6002 (2020).
- [55] A. Semenov, G. Gol'tsman, and R. Sobolewski, *Superconductor Science and Technology* **15**, R1 (2002).
- [56] G. Torrioli et al., *Optics Express*, **31**, 15942 (2023).
- [57] S. Barbieri et al., *Nature Photonics* **5**, 306 (2011).
- [58] F. Wang et al., *Laser & Photonics Reviews* **11**, 1770042 (2017).
- [59] P. Micheletti et al., *Science Advances*, in press (2023).
- [60] U. Senica et al., *Applied Physics Letters* **116**, 161105 (2020).
- [61] R. Wang et al., *ACS Photonics* **9**, 426 (2022).

Giacomo Scalari got his diploma in Physics at the Università di Pisa in 1999. After a period at Scuola Superiore S. Anna, Pisa, he completed his PhD at the Université de Neuchâtel in December 2005 with a thesis on magneto-spectroscopy and development of THz quantum cascade lasers. He moved to ETH in 2007 and in 2011 he became permanent senior scientist in the group of Prof. J. Faist. In April 2020 he was awarded the title of Professor from ETH Zürich. His research interests are in the field of THz ultrastrong light-matter coupling, where he pioneered the Landau polaritons platform, in THz quantum cascade lasers frequency combs and in THz metamaterials. He was awarded the Swiss Physical Society prize for Applied Physics in 2006 and an ERC Consolidator grant for researching THz quantum cascade lasers frequency combs in 2016.